

## Chapter 2

# Applications of XPS in Biology and Biointerface Analysis

Sally L. McArthur, Gautam Mishra, and Christopher D. Easton

**Abstract** XPS has been used extensively to characterize the surface chemistry of materials used in bioengineering and is increasingly finding a role in biology. Its ability to characterize both the elemental and chemical structures of the surface makes it particularly useful, as it can be used to identify and image the chemical functional groups present on the surface of virtually any material. This review is intended both to profile traditional applications of XPS in bioengineering and biology as well as to discuss advances in XPS instrumentation aimed at enabling the characterization of biological and organic materials.

## 2.1 Introduction

The past 15 years have seen a rapid rise in techniques capable of probing both biology and its interface with materials. Techniques such as surface plasmon resonance (SPR), optical waveguide lightmode spectroscopy (OWLS), and quartz crystal microbalance (QCM) are all used to give insight into the kinetics of protein–protein interactions and the interactions that occur between biomolecules and materials. Atomic force microscopy (AFM) can be used to image single molecules, unfold proteins, monitor surface topography, and measure the forces that hold biological structures together. While all of these techniques give invaluable

---

S.L. McArthur (✉)

Biointerface Engineering Group, IRIS, Faculty of Engineering and Industrial Sciences,  
Swinburne University of Technology, Hawthorn, VIC 3122, Australia  
e-mail: SMcArthur@swin.edu.au

G. Mishra

Kratos Analytical, Wharfside, Trafford Wharf Road, Manchester, M17 1GP, UK

C.D. Easton

CSIRO Molecular and Health Technologies, Bag 10, Clayton South, VIC 3169, Australia

insight into specific biological processes, none of them provides chemically specific information. To fill this gap in our knowledge, surface chemical analysis techniques more commonly associated with pure materials science have been applied to study both biological events and the interactions that occur at the interface between biology and engineering.

X-ray photoelectron spectroscopy (XPS), also called electron spectroscopy for chemical analysis (ESCA), is the most widely used ultrahigh-vacuum (UHV) surface analysis technique. In an XPS experiment, the sample is placed in a UHV chamber and irradiated with X-rays of a specific wavelength. The adsorption of the X-rays by atoms in the sample leads to the ejection of core and valence electrons (photoelectrons). These photoelectrons have energies that are unique to each element and sensitive to their chemical states. Significantly, the intensities of the photoelectrons are proportional to the concentration of the element from which they are ejected. Of course, X-rays are capable of penetrating the sample surface up to many micrometers, but a small fraction of the photoelectrons generated relatively close to the surface (~10 nm) have sufficient energy to escape into the vacuum system without being scattered. These are the photoelectrons that are detected in XPS.

There are a number of key characteristics that make XPS suitable for the analysis of biological materials and biointerface analysis, which we discuss next.

### ***2.1.1 Range of Elements Analyzed***

XPS detects all elements except H and He. In general, for the detection of proteins, the nitrogen content of the protein is utilized to determine the presence and quantify the amount of protein on a surface [1]. The presence of nitrogen in the substrate can complicate quantification; however, monitoring other elements that are present in the protein and not in the substrate (such as Fe, Zn, or S) can overcome this complication. In addition, if the substrate contains an element not found in the protein, signal attenuation may be used to quantify the amount of adsorbed or immobilized protein. Similar approaches can be utilized to detect other biomolecules, including DNA [2], lipids, and mucins [3]. Critically, XPS can be used in the detection of adventitious contaminants such as silicones, hydrocarbons, and other chemical species that may affect the biological interactions or the function of a biomaterial or medical device [4].

In addition to detecting elements, XPS can be used to characterize specific functional groups associated with a specific element. For carbon,  $\text{CH}_x$ ,  $\text{C-O}$ ,  $\text{C=O}$ , and  $\text{O-C=O}$  may all be differentiated due to variations in the functional group's electronegativity, shifting the relative energy of their ejected photoelectron. In some instances, the binding energy differences between some functional groups are too small to be resolved clearly by XPS; however, chemical derivatization can be used to overcome this problem. In this case, the functional group is tagged with a unique element that has a high photoionization cross section and is stable in the analysis conditions, such as F or Br [5]. Common compounds utilized include trifluoroacetic

anhydride for hydroxyl tagging [6], trifluoroethanol for carboxyl groups [7], and pentafluorobenzaldehyde for amine detection [8]. Independent of complications associated with small shifts in binding energy, derivatization also enables the identification and quantification of the functional group present at the interface (e.g., acids or amines) and can be used to assess relative activities in specific applications or reaction conditions [7, 9].

### 2.1.2 Surface Sensitivity

XPS is a surface-sensitive technique because it monitors unscattered photoelectrons, approximately 95% of which arise from within a distance of three times the inelastic mean free path ( $3\lambda$ ) of the element being detected. For carbon, with  $\lambda = 3.3$  nm, this means that the XPS sampling depth is  $\sim 10$  nm when the sample surface is positioned normal to the detector. It is the sampling depth for carbon that is commonly quoted as the XPS sampling depth. This means that the sampling depth is larger than the dimensions of many adsorbed proteins and biomolecules. This allows for signals from a substrate and an adsorbed (i.e., protein) overlayer to be detected simultaneously.

Attenuation of a specific element from the substrate, or the introduction of a specific element by the adsorption of a protein, can be utilized to calculate the adsorbed film thickness or determine the intercalation of protein into a porous substrate. Algorithms utilizing the X-ray emission angle ( $\theta$ ), theoretical composition of the protein film or substrate ( $I_\infty$ ), and inelastic mean free path of the emitted photoelectron of a specific element ( $\lambda$ ) enable the calculation of the protein film thickness ( $d$ ) using Eq. 2.1.

**Equation 2.1**, XPS overlayer algorithm.

$$I = I_\infty \exp^{-d/\lambda \cos \theta} \quad (2.1)$$

A number of other algorithms exist, but most assume that the protein film is homogeneous and continuous. If the XPS data do not fit the form of Eq. 2.1, this indicates that the protein film is incomplete or patchy. Paynter and Ratner have shown that it is possible to incorporate a fractional coverage term into Eq. 2.1, but the quantity of protein adsorbed to the surface must be established from another technique, such as radiolabeling [10].

### 2.1.3 Angle-Dependent XPS (ADXPS) and Depth Profiling

As stated earlier, the sampling depth of XPS is dependent on the inelastic mean free path of the emitted photoelectron of the specific element ( $\lambda$ ) and the X-ray emission angle ( $\theta$ ) via Eq. 2.2.

**Equation 2.2**, XPS sampling depth.

$$d = 3\lambda \cos\theta \quad (2.2)$$

Thus, by varying the angle between the X-ray source and the sample by simply tilting the sample stage, one can vary the XPS analysis depth from ~2 to 10 nm, depending on the element being analyzed. ADXPS enables the detection of compositional variations as a function of depth from the sample surface in a nondestructive fashion and allows the continuity and depth distribution of the coating to be probed.

Traditionally, ion beam depth profiling of materials in XPS has been limited to inorganic materials due to ion beam-induced sample damage. In recent years, there have been significant developments in the ion sources for depth profiling of organic materials. Driven by the ToF-SIMS community, cluster ion sources (including  $C_{60}^+$  [11] and coronene [12]) have become available for integration into XPS instruments. While the use of these sources is still in its infancy for biology, they have been successfully implemented to explore drug distributions in pharmaceuticals [12] and depth profiling of organic materials [13].

### 2.1.4 *Freeze Hydration XPS*

As many of the materials used in bioengineering and all biomolecules operate in a hydrated environment, questions about the relevance of XPS data to bioengineering applications and biological interactions are often raised [14, 15]. Freeze hydration XPS, developed by Lewis and Ratner in the early 1990s [16], involves the rapid freezing of a wet sample within the XPS entry chamber and can be used to both circumvent and investigate issues associated with sample dehydration. Once a sample is frozen, subsequent exposure to UHV at a temperature of approximately  $-100\text{ }^{\circ}\text{C}$  etches the ice from the surface via sublimation. The sample temperature is then lowered below  $-120\text{ }^{\circ}\text{C}$  for XPS analysis. Both the study by Lewis [16] and a number of subsequent investigations [17, 18] have shown that “freeze hydration” XPS enables the hydrated surface chemistry of polymers to be probed and the processes of polymer reorganization at interfaces investigated.

There were a number of XPS protein adsorption studies using cryogenic sample preparation that predate the work by Lewis and Ratner and investigated the role of substrate chemistry in the distribution and orientation of protein films [19, 20]. A review of the more recent literature illustrates that there has been very little work on biological or bioengineering applications published since 1993. The work that has been published has focused on the analysis of bacterial cells and cell membranes [21]. Some of this may be due to the complex nature of the sample preparation and the extended amount of instrument time required in preparing for and performing the experiments. In addition, as noted by Lewis, surface contamination is a major issue as cryogenic temperatures increase the rate of condensation of contaminants onto the sample surface in both air and vacuum [16]. As cryogenic sample preparation becomes more commonplace for the ToF-SIMS analysis of biological samples, there may be renewed interest in cryogenic XPS.

### 2.1.5 XPS Imaging and Mapping

The increasing interest in spatial control of cells and biomolecules for applications such as tissue engineering and array technologies has seen the requirement for small spot analysis and chemical state imaging move to the forefront of XPS research. Recent advances in instrumentation have seen the spatial resolution of XPS imaging improve significantly. Today, imaging can be achieved with spatial resolutions below 10  $\mu\text{m}$  as the standard; in some cases, a near-micron resolution can be achieved [22]. A number of groups have used standard spot size analysis ( $300 \times 700 \mu\text{m}$ ) to characterize both chemical and thickness gradients over relatively large areas ( $\sim 10 \text{ mm}$ ) [7, 23], producing two- and three-dimensional maps of the material. Unlike ToF-SIMS, quantitative XPS imaging is also possible. While the process is not trivial, there are an increasing number of papers being published that detail methods for both producing and processing quantifiable images [24–26].

This chapter aims to explore the increasing number of areas where XPS is applied to address issues in biology and its engineering cousin, bioengineering. After an introduction to the instrumentation involved, we will focus on a number of the specific applications where XPS is in use today to investigate biological processes and the interface between materials and biology.

## 2.2 Instrumentation

XPS instrumentation has advanced significantly in the last three to four decades, largely driven by the demand of quantitative surface analysis in the fields of catalysis [27, 28], microelectronics [29–31], corrosion science [32, 33], and biomaterials [34–36]. In most common cases, the samples studied by this surface analysis method are durable and robust. When interest developed in applying XPS to organic and biological systems, special instrument designs and experimental considerations were needed. In particular, concerns about the effect of the ultrahigh-vacuum environment on traditionally hydrated biological surfaces needed to be addressed. Alongside this, issues including X-ray and electron damage, surface charge accumulation, narrow X-ray line widths required for higher energy resolution and finer chemical discrimination, high sample throughput, and better signal-to-noise ratios needed to be addressed. Advances in instrument manufacturing and the availability of cutting-edge electronics led to the development of instruments that are precisely tuned to address many of these specific issues. Nowadays, monochromatic X-ray probes are standard in most commercial laboratory instruments, with a probe diameter down to less than 10  $\mu\text{m}$ . The energy resolution and signal-to-noise ratio of the analyzer system have improved with the introduction of position-sensitive multi-channel detectors. Imaging analyzers and sophisticated lens systems, such as a magnetic immersion lens, have contributed significantly to the improvement in small-area imaging XPS performance and, most importantly, surface charge

neutralization. A 1–3- $\mu\text{m}$  chemical state image resolution can now be routinely achieved on a laboratory XPS instrument, thus enabling researchers to examine small features often studied in the fields of biology and medicine.

### **2.2.1 Overview of XPS Instrumentation**

Most commercial XPS systems are divided into two main chambers, one in which the XPS analysis is carried out (sample analysis chamber, or SAC). This is directly linked to a second chamber (sample entry chamber, or SEC), a sample introduction chamber consisting of anything from a simple introduction vacuum lock or a more complicated vacuum lock with other specialized preparation or treatment equipment attached to it. Stepper motor-controlled automatic or manual mechanisms are available to transfer the sample from one chamber to another.

As shown in Fig. 2.1, the sample introduction chamber is usually pumped by turbomolecular pumps capable of attaining vacuum levels of  $\sim 5 \times 10^{-8}$  Pa (or  $\sim 5 \times 10^{-10}$  mbar). Roughing and backing of the turbomolecular pumps are provided by well-trapped rotary pumps, although novel “dry” backing and roughing pumps such as diaphragm and scroll pumps are now becoming more common, particularly where hydrocarbon contamination must be avoided. The sample is introduced directly into the load lock by venting this chamber to dry nitrogen. For more complicated load lock designs, often the sample is introduced, as shown in Fig. 2.1, in a relatively smaller chamber (often referred to as fast-entry load lock), where specific treatments, such as sample cooling, are performed. Temperature measurements are made by a thermocouple in direct contact with the sample stub in the introduction chamber. Once a good level of vacuum is achieved, the sample is then transferred into the main analysis chamber or other attached preparation or treatment chambers. The use of fast-entry lock arrangements allows the main load lock to remain under ultrahigh vacuum at all times. The fast-entry lock arrangements can also be fitted with glove boxes for specialized sample treatment. Stainless steel is generally used for the vacuum lock and preparation chambers, although high-grade aluminum alloys are being used more, especially for locks. The sample-handling arrangement in the analysis chamber is also equipped with heating and cooling arrangements. The temperature is monitored by a thermocouple in direct contact with the sample stubs, and a feedback loop is used to program rates of heating and cooling. The temperature range for heating and cooling in the analysis chamber is typically in the range of +600 to  $-150^\circ\text{C}$ .

The samples are often transferred between the introduction and analysis chamber by using an automated or manual sample insertion probe. Various vacuum interlocks operate between the connecting chambers in a fail-safe mode to prevent loss of UHV conditions.

The SAC is generally constructed of mu-metal for effective magnetic screening and is designed with numerous vacuum ports that have a “line of sight” to the

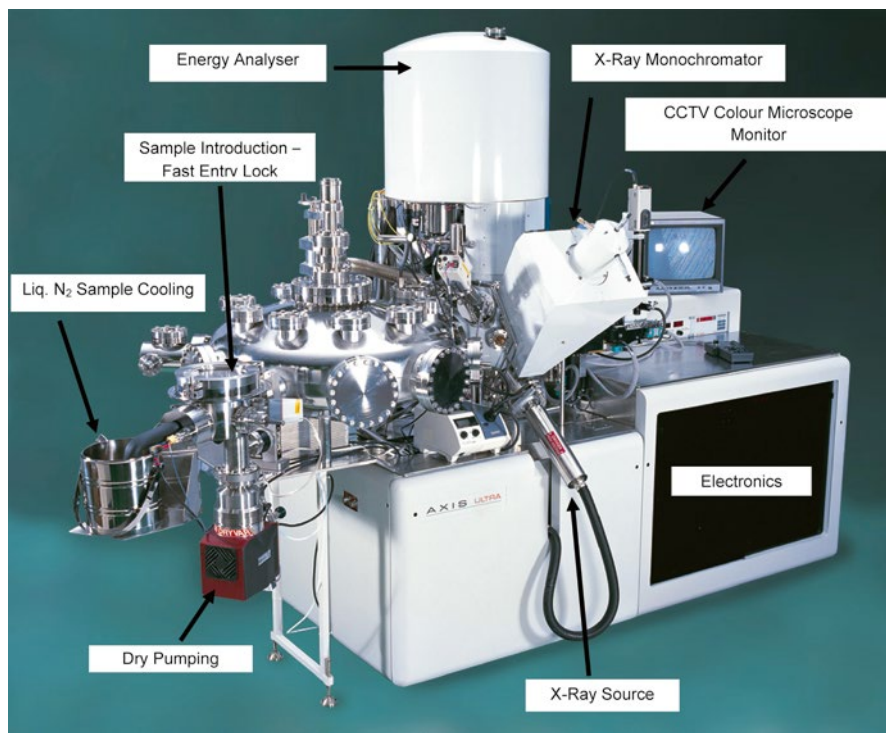


**Fig. 2.1** An example of a commercial XPS instrument—the Kratos Axis Ultra DLD. This version of the instrument has been fitted with a radial distribution chamber (RDC) permitting the transfer of a sample to and from other equipment under vacuum. The computerized user interface is not shown in this figure (Reproduced with permission from Kratos Analytical Ltd.)

sample in order to accept a comprehensive set of accessories, including ion guns. The analysis chamber is generally pumped by ion and titanium sublimation pumps, and the pressure is maintained below  $\sim 1 \times 10^{-8}$  Pa during analysis.

### 2.2.2 Charge Neutralization

As discussed earlier, the basic XPS experiment involves bombardment of a material in vacuum with soft X-rays that are capable of penetrating the sample surface up to many micrometers. Absorption of X-ray energy by an atom in a solid leads to ejection of an electron, in a process termed “photoionization,” from either from the core level or valance bands. A small fraction of these photoelectrons generated relatively close to the surface (depth  $\sim 10$  nm) have sufficient energy to escape into the vacuum system (i.e., photoemission); the process is termed the “photoelectric effect.” The photoelectric emission is the energy analyzed to produce a signature spectrum of electron intensity as a function of energy.

For a conducting sample, conservation of energy leads to the following equation:

$$E_k = h\nu - E_B^F - \phi_{sp}$$

where  $E_k$  is the measured kinetic energy of the emitted photoelectron,  $h\nu$  is the energy of the exciting X-ray photon,  $E_B^F$  is the electron binding energy relative to the Fermi level ( $E^F$ ) of the sample, and  $\phi_{sp}$  is the work function of the spectrometer. Since the binding energy is generally of interest to the user, the spectrometer is set up to record the spectrum on this energy scale directly.

For insulating samples that do not have a well-defined Fermi level, and to deal with uncertainty in surface potential developed by emission of the photoelectrons, we modify the above equation as

$$E_k = h\nu - E_B - \phi$$

where  $\phi$  is now the term that captures these surface potential uncertainties and the actual reference point for  $E_B$ . If the binding energies for different insulating samples are to be meaningfully compared, a common reference point needs to be established. For polymers, biological samples, and organic samples, the hydrocarbon component (C–C/C–H) of the C 1s peak is typically set to 285.0 eV and used as an internal reference.

Non-monochromatic XPS instruments do not generally require a dedicated charge compensation system. The X-ray flux in these systems is relatively uniform, and there are usually enough secondary electrons in the vicinity of the sample induced by the X-ray beam's striking the X-ray window and the spectrometer surface to produce adequate charge compensation.

For monochromatic XPS systems, two major advances in charge compensation systems are commonly available in commercial instruments. The first operates with spectrometers using a magnetic immersion lens often referred to as a “snorkel lens” [37]. The magnetic field intersecting the sample traps photoemitted electrons, causing them to spiral about the field lines. The charge balance plate causes lower-energy electrons to be reflected back to the sample, greatly reducing the number of additional electrons needed to reach equilibrium. As all of the reflected electrons come from the sample, the surface never becomes overcharged. The design of the neutralizer enables excess electrons to become trapped in the magnetic field until required for the neutralization process. This creates a sufficiently high flux of electrons and ensures that the whole analyzed area has a uniform surface charge, providing optimal XPS performance. A second approach of charge compensation relies on the use of a low-energy ion beam for neutralization. A stream of low-energy ions discharges the peripheral regions of the sample, and so electrons from the flood gun are not reflected before they can reach the illuminated area. In absence of the ion flux, the sample surface approaches the potential of the most energetic electron striking it, thus producing an unstable, repulsive potential. This process ensures that the potential of this peripheral region, which can be charged several volts negative, is kept close to the potential of the illuminated region so more flooding electrons can



reach the illuminated region. When the ion beam energy has been kept below 50 eV, little or no sample damage or implantation has been observed. It has also been shown that by using a low-work-function metal oxide cathode in the flood gun, a narrow energy distribution of flooding electrons can be used, making the potential across the illuminated region more uniform [38].

Biological samples can often have surface topography, and this can be a major issue for charge compensation. In the case where collimated low-energy ion beams are used, one would only expect partial neutralization of the sample surface, because of surface roughness and shadowing effects. This can be overcome using a magnetic immersion lens system, as the spiral trajectory of the neutralizing electrons allows them to evenly reach the sample's surface irrespective of topography.

### 2.2.3 Depth Profiling

As discussed earlier, the sampling depth achieved by XPS is approximately 10 nm. However, it is common to have samples composed of a much larger ( $>10$ -nm) compositional gradient. Furthermore, the chemical information generated from the top  $\sim 10$  nm is a convolution of information from all the layers contained within this region. The chemical distribution as a function of depth from the outermost  $\sim 10$  nm of the surface can be converted into depth profiles by using data acquired in an angular-dependent XPS (ADXPS) experiment. A number of different algorithms exist, but many, like that shown in Eq. 2.2, assume that the overlayer is homogeneous and continuous. More realistic models that do not rely on oversimplifying assumptions exist (e.g., Tougaard [39, 40]) and allow noncontinuous coatings and nanostructured surfaces to be characterized. Compositional depth profiles can also be established using these methods. By combining ARXPS with  $^{125}\text{I}$  radiolabeling, the homogeneity and distribution of protein on the surface can also be assessed. If the surface is porous, the distribution of protein *within* the outer 10 nm of the material may also be monitored. Paynter produced an algorithm for biological systems in the early 1980s [10], and software is now readily available for producing depth profiles from ARXPS data (e.g., The National Physics Laboratory (NPL) ARCTick firmware available from <http://www.npl.co.uk/nanoanalysis/arctick.html>).

To investigate chemical distributions at greater depths (i.e., more than 20 nm from the top surface), destructive depth profile experiments (i.e., ion etching) are performed. Conventionally in this approach, monoatomic ions such as  $\text{Ar}^+$  or  $\text{Cs}^+$  are used to etch a few nm (2–10 nm) of the sample surface, and the bottom of the etching crater is analyzed at regular intervals. Although this depth profile approach was found to be very useful for inorganic systems, application in the field of organic, polymer, and biological materials is limited, as the structural information of the organic systems is very susceptible to damage from the monoatomic ion beams. The accuracy of analysis is further compromised by intermixing and knock-in of atoms at the bottom of the crater. Recently, it has been shown that minimally destructive XPS depth profiles of organic materials can be obtained by sputtering with large cluster ions beams (e.g.,  $\text{C}_{60}$  [11], coronene [12]).

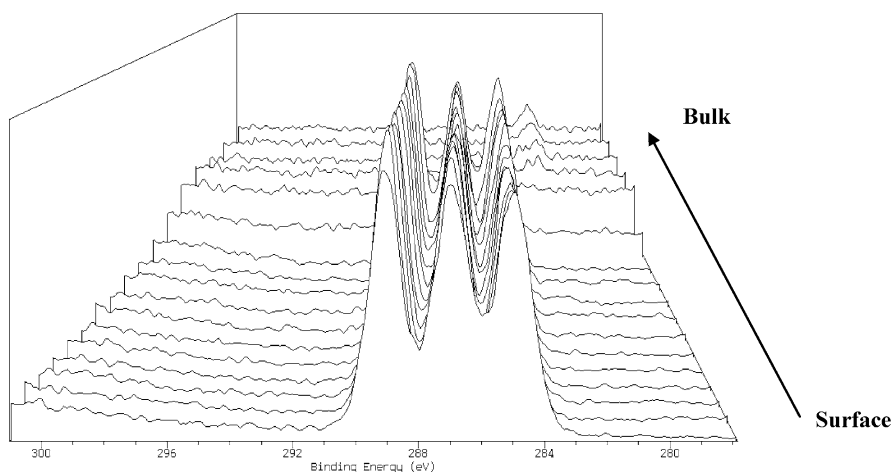


**Fig. 2.2** The C 1s spectra of spun-cast PLGA during a depth profile experiment using the coronene gun developed by Kratos

Coronene – ( $C_{24}H_{12}$ ) is a polycyclic aromatic hydrocarbon (PAH) consisting of six carbon rings. Within the ion gun, coronene powder is loaded into the oven assembly and heated to sublime coronene molecules into the gas phase. Coronene vapor passes into the source region and is ionized by electron-impact ionization. Coronene ions are formed into a beam by the condenser lens and projected into a high-resolution Wien filter to mass/energy-select a specific ion species. The ion gun is designed to operate with ion acceleration voltages up to 20 keV, but the voltage may be set to choose either singly or doubly charged ions. If doubly charged ions are selected, then the effective ion energy available can be increased to 40 keV.

Results show that organic systems can be successfully depth-profiled using the coronene cluster ion beam. Success is defined in terms of two requirements: (1) a depth profile with a constant etch rate through the sputtered layer; and (2) a minimum amount of chemical damage to the sample during the sputter depth profile. Model polymers [e.g., PLGA, poly(lactic-co-glycolic acid)] spun-cast onto silicon substrate (thickness – 85 nm) were used to better understand the performance of this cluster ion gun on organic systems. C 1s spectra recorded at regular intervals during coronene depth profile are shown in Fig. 2.2. Prior to exposure to the coronene source, three distinct chemical environments were detected in the C 1s spectrum, a hydrocarbon peak at 285.0 eV, a carbon singly bonded to oxygen peak at 286.8 eV and a C peak for the ester group at 289.2 eV. During the coronene profile (16-keV beam energy), the chemical structure of the polymer was found to be conserved throughout the film to the sample-substrate interface.

In another study, the coronene cluster ion source was used to study the distribution of a model drug codeine ( $C_{18}H_{21}NO_3$ ) in poly(L-lactic) acid matrix as a model for a drug-loaded polymer coating [12]. The controlled release of such active

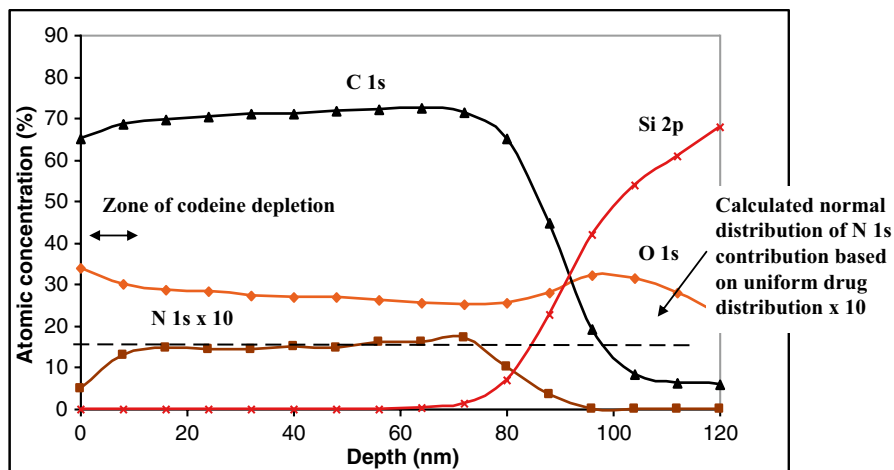


**Fig. 2.3** XPS depth profile from coronene-etched drug-loaded PLA film showing C 1s, O 1s, N 1s $\times$ 10 and Si 2p signal and calculated nitrogen concentration assuming a uniform drug distribution through the film thickness. The N 1s signal was used as a unique indicator for the presence of drug in the sample (Reprinted with permission from Ref. [12]. Copyright © Elsevier Ltd. 2009)

pharmaceutical ingredients from polymers over prolonged periods of time is vital for their application in drug-eluting stents and other drug-loaded delivery devices. Figure 2.3 shows the coronene ion depth-profile data from the drug–polymer binary system where the N 1s signal was used to monitor the distribution of the drug as a function of depth. XPS analysis of the bottom of the sputter crater with sputter time indicated that codeine was depleted from the surface and segregated to the bulk of the polymer films by comparison with a uniform distribution calculated from the bulk loading. This serves to illustrate that surface depletion of drug occurs, which poses important implications for drug-loaded polymer delivery.

## 2.2.4 Small Spot Spectroscopy

It is often necessary to analyze a small feature of interest on the surface of a specimen. For the analysis to be effective and accurate, the signal from the surrounding area should be eliminated. Two main approaches are used in current research-grade instruments to achieve this.

The first approach relies on flooding the sample with X-rays but limiting the area from which the photoelectrons are collected, generally by using the transfer lens. In most spectrometers, the electron optic lenses are fitted to the analyzer and operated in a way to produce a photoelectron image at some point in the electron optical column. By placing a small aperture at this point, only the electrons emitted from a defined area are allowed to pass through the aperture and reach the analyzer.

Usually in these instruments, a choice of aperture is available for selection, thus enabling analysis from a wide range of areas. Another variant of this instrument uses an iris to provide a continuous range of analysis areas. Quite often fixed apertures or an additional iris is positioned in the lens column to correct for spherical aberrations in the electron optical system by limiting the acceptance angle of the lens. Using this technique, commercial instruments can provide small-area analysis down to about 10  $\mu\text{m}$ .

In the second approach, a monochromatic beam of the X-ray is focused into a smaller area to analyze the feature of interest on the sample surface. Here, a quartz crystal is bent so that it can focus a beam of X-rays and provide monochromatic X-rays by diffraction. In this respect, it behaves rather like a concave mirror. The focusing is usually achieved using a magnification of unity, which means that the size of the X-ray spot on the specimen is approximately equal to the size of the electron spot on the X-ray anode. Analysis areas down to about 10  $\mu\text{m}$  can be achieved in commercially available instruments using this method.

### ***2.2.5 XPS Imaging and Mapping***

Another area where XPS instrumentation has improved significantly is photoelectron imaging. Manufacturers use two distinct approaches to obtain XPS maps: serial acquisition, in which each pixel of the image is collected in turn (mapping mode); and parallel acquisition, where data from the entire analysis area is collected (direct or real-time imaging).

Serial acquisition of images is based on a 2D rectangular array of small-area XPS analysis. In this approach, the micro-focused beam of X-rays is scanned over the sample and an image is built one pixel at a time in a point-by-point acquisition. The ultimate spatial resolution of the image is thus determined by the size of the smallest analysis area. Typically, the spatial resolution obtained by this method of image acquisition is limited to the focus of the X-ray beam, such as  $\sim 10\ \mu\text{m}$  based on 80–20 % (or 84–16 %) edge resolution measurements. Serial acquisition is generally slower than the parallel acquisition but has the advantage that one can collect a range of energies.

In parallel acquisition of photoelectron images, the entire field of view is imaged simultaneously without scanning voltages being applied to any component of the spectrometer (imaging mode). Obtaining images in this way requires additional lenses in the spectrometer and the use of a 2D detector in the image plane. The image resolution has been significantly improved by limiting the angular acceptance of the lens, thus reducing spherical aberrations. The use of a magnetic immersion lens in the specimen region also reduces aberrations and therefore allows higher sensitivity at a given resolution. This method of imaging is relatively fast; commercial instruments can produce images with an image resolution as low as 3  $\mu\text{m}$ .

Parallel imaging clearly provides better image resolution and is faster than the serial methods, but it collects an image at a single energy only. Obtaining more

accurate image measurements using the parallel image acquisition mode thus requires a second measurement at some energy remote from the peak, where the signal intensity is approximately equal to the estimated background signal under the peak maximum. By mathematically subtracting the background signal from the signal at the peak's maximum, we can routinely make more accurate measurements.

## 2.3 Characterization of Biomolecules

### 2.3.1 *Proteins and Peptides*

A significant amount of work exists on the use of XPS to study proteins. Due to similarities in the chemical composition of most proteins, XPS cannot be used to differentiate individual components within a complex mixture of proteins. Coupled with the fact that analyzing these biomolecules requires them to be immobilized onto a surface, which can contribute to the analyzed spectra, XPS is not ideal for a fundamental chemical analysis of proteins and peptides. The strength of XPS is realized when applied to examine the immobilization of these biomolecules onto surfaces. Fundamental knowledge of the adsorption process of proteins to surfaces at the molecular level is vital for the development of interfaces that exhibit specific biophysical properties [41]. XPS provides the opportunity to examine adsorbed proteins and elucidate information regarding the orientation, surface coverage, and layer thickness [1, 10, 42].

Proteins are composed of mostly carbon, oxygen, and nitrogen and can contain low levels of other elements, including sulfur, phosphorus, and metals. Detection using XPS is typically achieved by monitoring changes in the nitrogen signal and attenuating the substrate signal. The highest sensitivity to protein adsorption can be achieved on nitrogen-free substrates or in situations where the substrate is rich in an element not found in the protein, such as fluorine. Biochemical assays, such as radiolabeling using  $^{125}\text{I}$  or detection using a fluorescent or enzyme-labeled antibody, are often used in conjunction with XPS to provide a complete picture of the absorption characteristics of the system under examination [1, 43, 44]. Figure 2.4 demonstrates the correlation of  $^{125}\text{I}$  data with XPS results, for the adsorption of fibrinogen onto mica [1]. These results compare the XPS detection limit for proteins as calculated by using the At% N signal (open circles) or attenuation of a unique substrate signal (Al) shown here as the N(1s)/Al(2s) ratio ( $x$ ). In both cases, the detection limit for the protein is shown to be  $\sim 10 \text{ ng/cm}^2$ . Much of the early work and related theory about the detection of proteins has been summarized by Paynter and Ratner [45] and updated in papers by Castner and Ratner [42] and Wagner et al. [1].

Even when the substrate contains nitrogen, it is still possible to detect protein although the limits of detection are reduced. Figure 2.5 shows the high-resolution C 1s spectrum of a nitrogen-containing plasma-polymerized heptylamine thin film (HApp) before (solid line) and after the adsorption of IgG (dashed line). While the

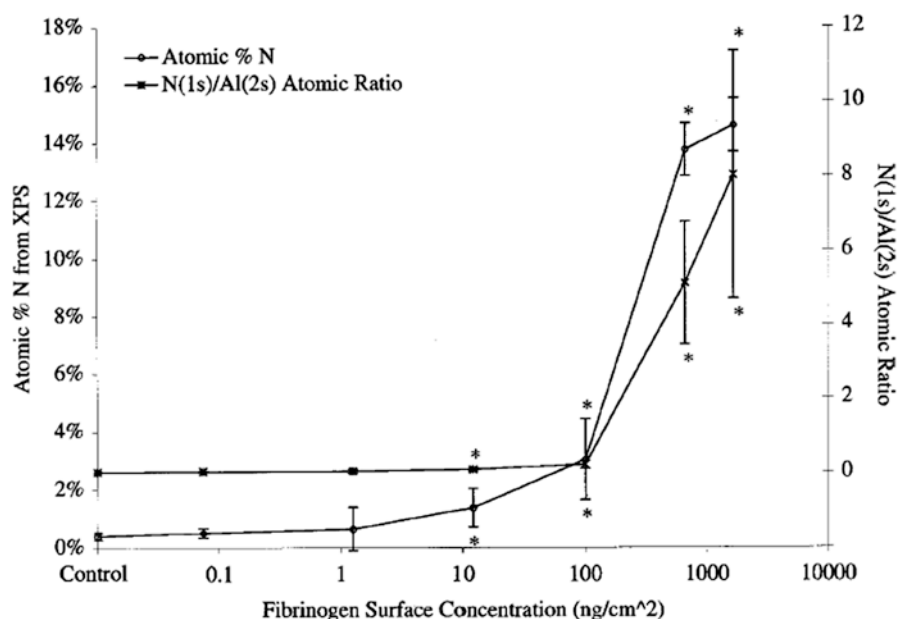


**Fig. 2.4** Surface nitrogen detected by XPS analysis of fibrinogen adsorbed onto mica. N/Al atomic ratios are also given for mica. Asterisks (\*) indicate samples that are significantly different from the control samples ( $p \leq 0.01$ ) (Reprinted with permission from Ref. [1]. Copyright © Koninklijke Brill NV 2002)

HApp contains nitrogen, it is in the form of amines and imines, whereas the protein contains amides as well as amines. XPS is able to differentiate between the amine and amide groups present on the surface, as the photoelectrons produced by the carbons found in these species have distinct energy shifts. The C–N related species are shifted to 286.5 eV, while the electronegativity of the amide (O–C–N) groups shifts the binding energy of the carbon associated with these groups to a higher binding energy of ~288 eV. Changes in the amine and amide content of the surface have been utilized to detect proteins on nitrogen-containing surfaces with a sensitivity of ~100 ng/cm<sup>2</sup> [1].

Peptides provide a simplified model system for examining protein adsorption processes to various surfaces. In addition, adsorbed peptides provide an opportunity to create a biologically specific interface for tissue engineering [46, 47] and bio-sensing [48]. As a result, there has been a significant increase in the research on peptide adsorption in recent years to surfaces such as gold, self-assembled monolayers, TiO<sub>2</sub>, sol–gel silica, and a range of polymers [46–53]. The analysis of peptides on surfaces creates its own challenges due to the size of the molecules and the often low density of their surface coverage. These factors combine to create what are often small changes in the chemical composition of a surface [46]. To some extent, ARXPS can be used to reduce the analysis depth and increase the relative

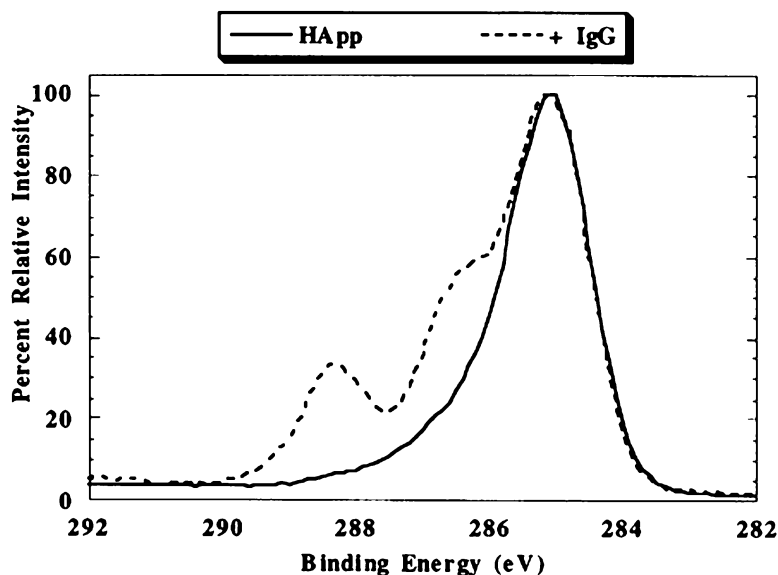


**Fig. 2.5** High-resolution XPS C 1s spectra recorded on a plasma-polymerized heptylamine (HA pp)-coated fluorinated ethylene propylene sample before (*solid line*) and after (*dashed line*) immersion in an IgG solution (Reprinted with permission from Ref. [43]. Copyright © Elsevier Ltd. 2000)

proportion of the surface chemistry that is due to the peptide, enabling the peptide to be differentiated from the substrate, which aids in limiting their impact on the surface chemistry [54]. An alternative approach is to use a process similar to derivatization to label the peptide with a specific chemical marker either prior to immobilization or once it is on the surface [48].

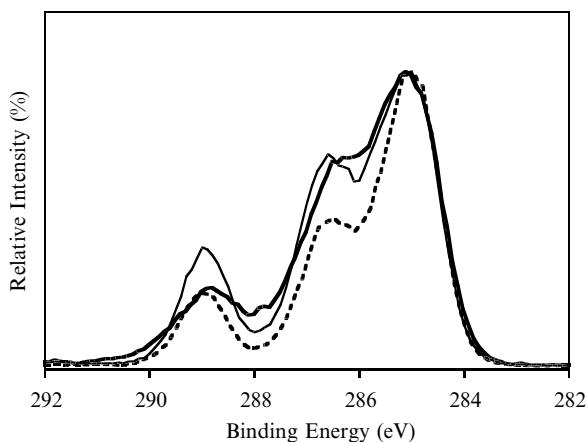
While the examples to date have been from model or laboratory systems, the same approaches have been used to implement XPS in the characterization of biomaterials and devices after *in vivo* experimentation [3, 55–58]. Table 2.1 presents the XPS atomic concentration data for Etafilcon A (Acuvue®) contact lenses before and after 10 min and 1 h of patient wear. These results show that a significant increase in nitrogen occurs after 10 min of wear, while after 1 h, a further increase in nitrogen in addition to oxygen was detected. An analysis of the high-resolution C 1s spectra from the lenses shown in Fig. 2.6 clearly demonstrates at 10 min the introduction of peak shifts associated with C–O/C–N species (~286.5 eV) and O–C–N species at 288 eV. After 1 h, the contributions have altered slightly again, with an increase in the O–C=O contributions at 289 eV, in line with the increased level of oxygen detected in the survey spectrum. From this data, researchers deduced that the adsorption processes were initially dominated by proteins (e.g., after 10 min of wear), but as the wear time increased to an hour, oxygen-rich species (e.g., mucins or polysaccharides) adsorbed alongside the proteins [3].

**Table 2.1** XPS atomic concentrations of Etafilcon A (Acuvue®) contact lenses before and after wear for 10 min and 1 h. Numbers in parentheses are standard deviations (Reprinted with permission from Ref. [3]. Copyright © Elsevier Ltd. 2001)

	Atomic concentration (%)				Atomic ratios	
	C	O	N	Si	N:C	O:C
Unworn ( $n=4$ )	72.5 (1.2)	27.0 (1.6)	0.4 (0.2)	0.1 (0.1)	0.01 (0.00)	0.37 (0.03)
10 min ( $n=10$ )	72.6 (2.3)	24.5 (2.7) <sup>a</sup>	2.3 (0.8) <sup>a</sup>	0.1 (0.0)	0.03 (0.01)	0.34 (0.04)
1 h ( $n=8$ )	67.9 (1.0) <sup>a</sup>	28.2 (1.7) <sup>a</sup>	3.7 (1.6) <sup>a</sup>	0.2 (0.3)	0.05 (0.02)	0.42 (0.03)

<sup>a</sup>Indicates an atomic concentration statistically different from the unworn lens (Student *t*-test,  $p < 0.01$ )

**Fig. 2.6** High-resolution XPS C 1s spectra from an Etafilcon A (Acuvue®) contact lens before (dotted line) and after 10 min (solid line) and 1 h of wear (thin line) (0° take-off angle) (Reprinted with permission from Ref. [3]. Copyright © Elsevier Ltd. 2001)



### 2.3.2 Other Biomolecules: Lipids, Mucins, Enzymes, and DNA

Proteins and peptides are not the only biomolecules that play a significant role in various biological processes. As a result, a number of studies have utilized XPS to detect and analyze the behavior of a range of biomolecules, including lipids [59–63], mucins and sugars [64, 65], enzymes [66–68], and DNA [2, 69–73]. Examining the chemical functionality and adsorption of these biomolecules to different surfaces is critical for advancing our fundamental understanding of their behaviors, developing bioarrays [2, 69–71, 73] and biosensors [66, 74], and controlling medical biofouling [3, 56, 75].

Table 2.2 demonstrates the elemental compositions of typical biomolecules [3]. From this data, it is apparent that adsorption of these biomolecules to a surface would induce a specific and measurable change in the surface composition of the substrate. As mentioned previously, a change in the nitrogen-to-carbon ratio (N:C) is often used as a detection marker for proteins, while a change in the oxygen-to-carbon ratio (O:C) is expected when lipids (ratio decrease) and mucins and sugars



**Table 2.2** Elemental compositions of common biomolecules (Reprinted with permission from Ref. [3]. Copyright © Elsevier Ltd. 2001)

	Atomic % composition			Atomic ratios	
	C 1s	O 1s	N 1s	N:C	O:C
Protein <sup>a</sup>	63.0	20.1	16.0	0.25	0.32
Protein <sup>b</sup>	65.3	18.1	14.2	0.22	0.28
Lipid <sup>c</sup>	95.0	5.0	0.0	0.00	0.05
Mucin <sup>d</sup>	58.0	31.0	9.8	0.17	0.53

<sup>a</sup>Theoretical composition of human albumin<sup>b</sup>Data derived from XPS spectra of thick human albumin film<sup>c</sup>Theoretical composition of cholesterol (C<sub>27</sub>H<sub>48</sub>O)<sup>d</sup>Data derived from XPS spectra of the glycosylated region of porcine submaxillary mucin (PSM, MUC1)

(ratio increase) adsorb to surfaces. The contrast between the adsorbed biomolecules and the substrate can be further enhanced using angle-resolved XPS (ARXPS), where the depth of analysis is varied to analyze a larger portion of the adsorbed or immobilized material.

The introduction of DNA microarray technology provides researchers a tool to study multiple cellular processes in parallel and thus is significant to fundamental biological research and biomedical applications [76–78]. In papers that have appeared between 2007 and 2009, Lee [2], Liu [69], and others [73, 78] have examined how XPS could be used to interrogate DNA arrays and provide a quantitative interpretation of DNA hybridization efficiencies and base-pair mismatch detection. Overlays of XPS images of phosphorus, nitrogen, and sodium onto the silicon image before and after hybridization from Lee's study clearly demonstrated an increase in signal intensity upon hybridization for microspots containing complementary probe sequences (Fig. 2.7) [2]. Liu's work was able to detect a single base mismatch as well as give valuable insight into hybridization efficiencies of the arrays [69]. These studies, together with others from groups around the world, have clearly demonstrated the applications of XPS in both the development and analysis of DNA arrays without the need for radioactive or fluorescent labels [73, 78, 79]. Significantly, many of these studies have also demonstrated the ability of XPS to detect variations and surface-induced problems within the hybridization processes of a wide range of commercial and noncommercial arrays [73, 79].

## 2.4 Cell, Bacteria, and Tissue Analysis

There are many types of cells, each containing a unique combination of components within the cell membrane, including phospholipids, proteins, glycosaminoglycans (GAGs), and cholesterol. XPS provides the opportunity to probe the cell surface and elucidate information regarding their composition and responses to environmental stimulation. As detailed earlier, all of the individual components of a cell have been

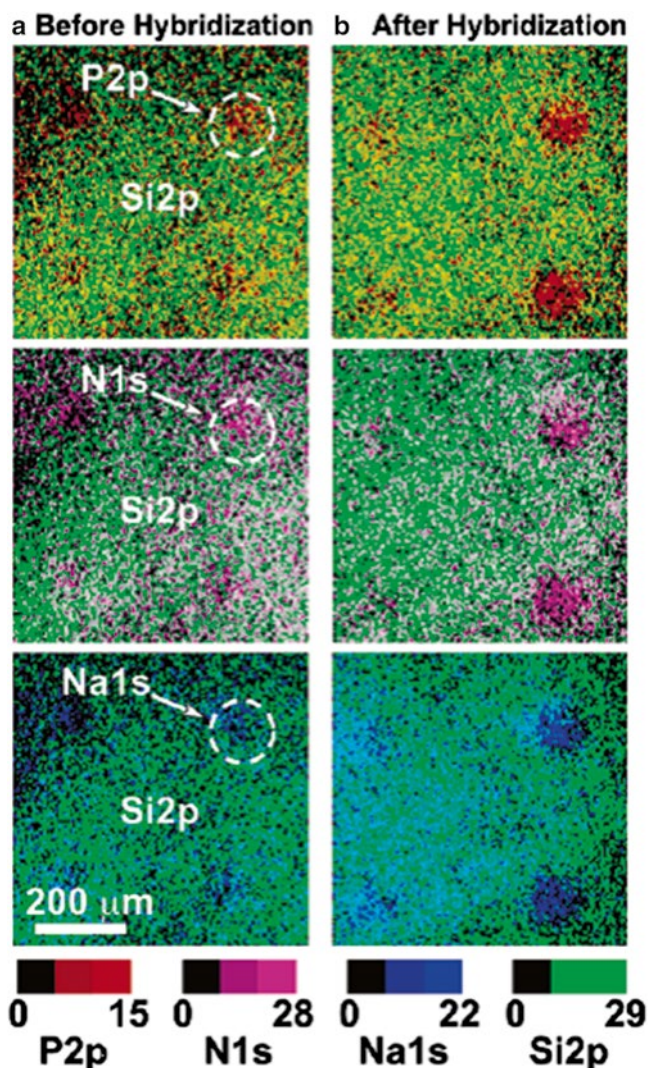


**Fig. 2.7** XPS overlay of phosphorus (P 2p), nitrogen (N 1s), and sodium (Na 1s) with the substrate silicon's (Si 2p) signal intensity images ( $800 \times 800 \mu\text{m}$ ) from printed DNA probes on CodeLink microarray slides (**a**) before and (**b**) after target hybridization (Reprinted with permission from Ref. [2]. Copyright © ACS 2007)

investigated on surfaces using XPS. When combined within a cell membrane, it becomes difficult to distinguish the individual components within the resultant XPS spectrum and quantitatively determine the amount of each component. As a result, the total element compositions obtained from survey spectra are typically employed to provide a semiquantitative comparison of cells [80]. In addition, the peak fitting

of high-resolution components (e.g., C 1s, N 1s, and O 1s) is typically undertaken. Postprocessing techniques can then be used to gain further insight. For example, the surface composition of bacteria can be modeled by three classes of components, specifically polysaccharides, peptides, and hydrocarbon-like compounds (lipidic compounds) [21].

The major focus of XPS analysis of cells has been in the investigation of microbial cells, including yeast, fungi, diatoms, and bacteria [81–84]. A number of studies have used XPS to explore changes in the chemical composition of the cell wall with changes in media (for suspended cells) or changes in substrate and media (for adhesive cells) [85, 86]. These types of studies are highly relevant for the minerals [87] and engineering industries, where specific microbial events are central to the success or failure of a process. In some instances, it enables industries to understand and prevent events such as biocorrosion [88–90], while in others it enables them to understand how surface characteristics of the bacteria or their extracellular polymeric substance (EPS) change in response to the environment [91, 92]. Properties that have been investigated include bacteria attachment and adhesion, with the aim of addressing biofouling [75, 85, 88], bioremediation [87, 93], and environmental applications [84, 94, 95].

An example of employing XPS to investigate the surface chemical structure of microbial cells is found in the work of Ahimou et al. [96]. The authors focused on the fitting of high-resolution peaks to elucidate the chemical functions of nine strains of *Bacillus subtilis*. Figure 2.8 presents high-resolution spectra of oxygen, nitrogen, and carbon for three *B. subtilis* strains. It is apparent that the spectral components assigned to the carbon peak vary considerably among strains, while the degree of variation is less significant for the nitrogen and oxygen peaks. Based on the peak position of the spectra components, the authors were able to determine the presence of individual components within the cell membrane. For example, the peak centered at 285 eV [carbon bound to carbon and hydrogen; C–(C,H)] was considered to originate from lipids or from side chains of amino acids, while the peak at ~289 eV (carboxylate and carboxyl groups) was the result of proteins and uronic acids. Further data interpretation of molar concentrations provided additional evidence; however, the authors did acknowledge that such modeling can lose significance as the number of unknown variables increases.

Another example of utilizing XPS to analyze *B. subtilis* was reported by Leone et al. [80]. In this study, a single strain (ATCC code: 6633) was analyzed using the standard freeze-dried technique and compared to frozen wet-paste samples suspended at different pH values. Applying this alternative sample-preparation technique allowed the authors to investigate protonation/deprotonation reactions of amine groups at the cell–water interface and elucidate information regarding the activity of the cell at specific pH values. It is interesting to note that different sample-preparation techniques were explored in this study, as the choice of sample-preparation and sample-handling techniques for XPS analysis of cells has long been a subject of some debate [14].

As XPS is a UHV technique, there has always been considerable concern as to whether the preparation techniques required and resultant dehydration disrupt the

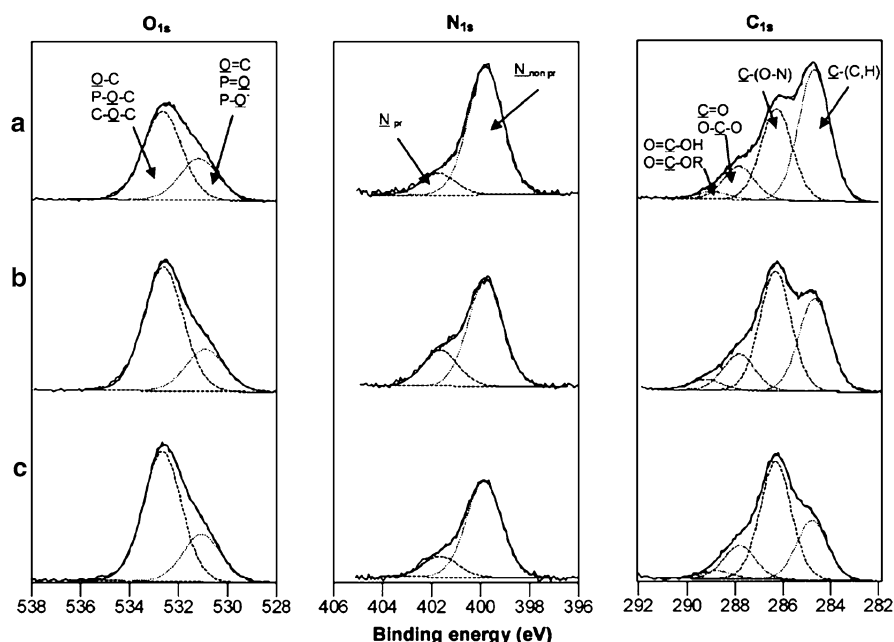


**Fig. 2.8** Representative O 1s, N 1s, and C 1s XPS peaks of three *B. subtilis* strains: (a) ATCC code: 7058; (b) ATCC code: 15476; (c) S 499 (Reprinted with permission from Ref. [96]. Copyright © Elsevier Ltd. 2007)

cell surface [14, 97]. In light of these concerns, a substantial amount of work has been undertaken to confirm XPS results by drawing comparisons with complementary data, including infrared absorption, water contact angle, and electrophoretic mobility, which are techniques that do not require ultrahigh vacuum [85, 86, 98]. These studies have shown a correlation between changes in the cell wall chemical composition with changes in the media or substrate and media, dependent on whether the cell was suspended or adhered to a surface prior to analysis. Despite these results, it is apparent that a significant amount of care must be taken when preparing microbial cells for XPS analysis. A number of reviews on the field exist and include critical assessment of the issues associated with sample preparation as well as details of the cell types that have been analyzed to date [14, 86].

### 2.4.1 Hard Tissue

Hard tissues include bone, dentin, cementum, and dental enamel; these represent the group of tissues that have undergone various degrees of mineralization during development. This mineralization is typically in the form of hydroxyapatite, which

is often applied as a biomaterial for bone implants. Within the literature, application of XPS to the analysis of hard tissue has focused on preventive and restorative dentistry. This has included analyzing the effects of various treatments, including laser irradiation [99, 100] and mouth rinses [101], and the effects of environmental exposure to chemical agents on the health of tooth enamel [102]. XPS has also been employed to examine bonding of materials and mechanisms of interactions between hard tissues and biomaterials [57, 103, 104]. In 2008, Lou et al. used XPS to investigate the surface chemical composition of 98 human maxillary first premolars to determine the compositional differences between right and left premolars [104]. The descriptive statistics of the percentage atomic concentration for all 12 elements detected were determined. The percentage of carbonate ( $\text{CO}_3$ ) was derived from high-resolution carbon spectra; the ratio  $\text{CO}_3/\text{P}$  is considered to be a measure of the susceptibility of enamel to acid attack. While no statistically significant difference was observed between right and left premolars, the authors considered the observed variation in  $\text{CO}_3/\text{P}$  potentially significant in terms of bond strength, as acid etching is typically performed prior to orthodontic bonding.

## 2.5 Biointerface Engineering

Biointerface engineering aims to bring together biology with surface engineering/science to unlock the fundamental properties driving biomolecule interactions with surfaces and to address key issues relating to biomaterials, tissue engineering, medical diagnostics, and many biotechnology applications, including sensors, bioarrays, and microfluidics. As XPS is a surface-sensitive technique, it is no surprise that it has become a core characterization tool within the discipline.

Differences between surface and bulk properties can arise via a number of different processes, including surface contamination, processing additives, blooming of plasticizers, and oxidation. Adventitious contaminants such as silicones and hydrocarbons can prevent adhesion of components, may influence the biological interactions of a biomaterial or tissue scaffold, and can interfere with the function of surface-immobilized proteins, peptides, and DNA. As such, it is critical that the surface chemistry of a material is verified at some point in the testing cycle prior to ascribing relationships between biological performance and surface chemistry or evaluating a specific immobilization strategy. There is a dearth of literature related to the detection of surface contamination via XPS, and a number of reviews exist that specifically focus on biomedical applications and issues [42, 105].

A key issue facing the integration of biomaterials is the stability of the surface when exposed to biological media; thus, an examination of how biological systems impact surfaces is paramount. XPS allows changes in the chemical composition of interfaces to be examined and has been used previously to examine the influence of microbiological corrosion (MIC) by marine aerobic bacterium on stainless steel [89] and the effects of cell culture medium on Ti, stainless steel, and a range of polymers, to name but a few examples [58, 106, 107].

As materials used in biology and bioengineering are often chosen for their mechanical or optical properties, there is an array of techniques and treatments designed to modify the material's surface for specific applications [42, 108]. Because the modifications are generally designed not to affect the bulk properties, the surface sensitivity of XPS is paramount, and angle-dependent XPS (ADXPS) is also regularly used to produce compositional depth profiles.

### ***2.5.1 The Future of XPS***

While XPS is a fundamental method for probing interfacial interactions in bioengineering, research is increasingly focusing on using XPS as part of a suite of characterization tools [42]. Obvious synergies exist between XPS and ToF-SIMS, as evidenced by the large number of papers currently in the literature that use both of these techniques. More fundamental insight into, and improvements in, devices and technology are progressively coming from combining UHV surface analysis with techniques commonly used in colloids and surface science (e.g., AFM[109]) and biological assays, such as ELISA [110], immunostaining [111], and polymerase chain reactions (PCR) [94]. This is where XPS can be used for its strengths in quantifying surface contamination, verifying surface chemistry [47, 109], and determining changes in surface chemistry after biological contact [94, 95, 111].

However, this is not to say that there are no opportunities for developments in XPS. Today multivariate statistical analysis (MVSA) routines are increasingly being developed today to assist in the interpretation of XPS data, particularly with results from imaging studies. Multivariate image analysis (MIA) methods such as scatter diagrams, principal component analysis (PCA), and classification methods are used to extract maps of pure components from degradation and images-to-spectra data sets [112]. Walton and Fairley have shown that by maintaining the relationship between images and spectra, it is possible to progress beyond the application of spectroscopic processing to multispectral imaging data sets, by utilizing the three-dimensional information contained in such data sets, to therefore improve both the processing and the visualization of the data [113]. With the ongoing development of depth profiling of biological materials being made possible by the introduction of the polyatomic ion guns, groups are just beginning to explore the applications of MVSA to explore biological systems. Studies from Artyushkova have used principal component analysis (PCA) to analyze quantitative XPS data, combining elemental and chemical species data as a function of sputter time to explore the structure of a yeast cell, with the final aim of exploring cell-directed assembly [113]. Of course, the ongoing close relationship between XPS and ToF-SIMS development will be of significant benefit as the sample-preparation techniques and cryogenic stages that have been developed for ToF-SIMS can be directly translated to XPS analysis.

## 2.6 Conclusions

Today XPS has established itself as a workhorse tool for biointerface analysis. While the key features of surface sensitivity and wide elemental analysis are at the heart of the technique, improvements in the imaging and depth-profiling capabilities of the instruments are increasingly drawing in new biological applications. But at the core, it is the relative ease of XPS data interpretation compared to ToF-SIMS and spectrometry techniques that will ensure that XPS retains its position well into the future.

## References

1. Wagner MS, McArthur SL, Shen MC, Horbett TA, Castner DG. Limits of detection for time of flight secondary ion mass spectrometry (ToF-SIMS) and X-ray photoelectron spectroscopy (XPS): detection of low amounts of adsorbed protein. *J Biomater Sci-Polym Ed.* 2002;13:407–28.
2. Lee CY, Harbers GM, Grainger DW, Gamble LJ, Castner DG. Fluorescence, XPS, and TOF-SIMS surface chemical state image analysis of DNA microarrays. *J Am Chem Soc.* 2007;129:9429–38.
3. McArthur SL, McLean KM, St John HAW, Griesser HJ. XPS and surface-MALDI-MS characterisation of worn HEMA-based contact lenses. *Biomaterials.* 2001;22:3295–304.
4. Foley JO, Fu E, Gamble LJ, Yager P. Microcontact printed antibodies on gold surfaces: function, uniformity, and silicone contamination. *Langmuir.* 2008;24:3628–35.
5. St John HAW, Gengenbach TR, Hartley PG, Griesser HJ. Surface analysis of polymers. In: O'Connor D, Sexton B, Smart RC, editors. *Surface analysis methods in material science.* Heidelberg: Springer-Verlag Berlin; 2000.
6. Beamson G, Alexander MR. Angle-resolved XPS of fluorinated and semi-fluorinated side-chain polymers. *Surf Interface Anal.* 2004;36:323–33.
7. Alexander MR, Whittle JD, Barton D, Short RD. Plasma polymer chemical gradients for evaluation of surface reactivity: epoxide reaction with carboxylic acid surface groups. *J Mater Chem.* 2004;14:408–12.
8. Ratner BD, Castner DG. Advances in X-ray photoelectron spectroscopy instrumentation and methodology: instrument evaluation and new techniques with special reference to biomedical studies. *Colloid Surf B.* 1994;2:333–46.
9. Whittle JD, Barton D, Alexander MR, Short RD. A method for the deposition of controllable chemical gradients. *Chem Commun.* 2003;14:1766–7.
10. Paynter RW, Ratner BD. The study of interfacial proteins and biomolecules by X-ray photoelectron spectroscopy. In: Andrade JD, editor. *Surface and interfacial aspects of biomedical polymers.* New York: Plenum Press; 1985. p. 189–216.
11. Chen Y-Y, Yu B-Y, Wang W-B, Hsu M-F, Lin W-C, Lin Y-C, et al. X-ray photoelectron spectrometry depth profiling of organic thin films using C60 sputtering. *Anal Chem.* 2007;80:501–5.
12. Rafati A, Davies MC, Shard AG, Hutton S, Mishra G, Alexander MR. Quantitative XPS depth profiling of codeine loaded poly(l-lactic acid) films using a coronene ion sputter source. *J Control Release.* 2009;138:40–4.
13. Yu BY, Chen YY, Wang WB, Hsu MF, Tsai SP, Lin WC, et al. Depth profiling of organic films with X-ray photoelectron spectroscopy using C-60(+) and Ar+ co-sputtering. *Anal Chem.* 2008;80:3412–5.



14. Pembrey RS, Marshall KC, Schneider RP. Cell surface analysis techniques: what do cell preparation protocols do to cell surface properties? *Appl Environ Microbiol.* 1999; 65:2877–94.
15. Vogler EA. On the biomedical relevance of surface spectroscopy. *J Electron Spectrosc Relat Phenom.* 1996;81:237–47.
16. Lewis KB, Ratner BD. Observation of surface restructuring of polymers using ESCA. *J Colloid Interface Sci.* 1993;159:77–85.
17. Lukas J, Sodhi RNS, Sefton MV. An XPS study of the surface reorientation of statistical methacrylate copolymers. *J Colloid Interface Sci.* 1995;174:421–7.
18. Magnani A, Barbucci R, Lewis KB, Leachscampavia D, Ratner BD. Surface-properties and restructuring of a cross-linked polyurethane-poly(amido-amine) network. *J Mater Chem.* 1995;5:1321–30.
19. Paynter RW, Ratner BD, Horbett TA, Thomas HR. XPS studies on the organisation of adsorbed protein films on fluoropolymers. *J Colloid Interface Sci.* 1984;101:233–45.
20. Ratner BD, Thomas TA, Shuttleworth D, Horbett TA. Analysis of the organisation of protein films on solid surfaces by ESCA. *J Colloid Interface Sci.* 1981;83:630–42.
21. Dufrene YF, VanderWal A, Norde W, Rouxhet PG. X-ray photoelectron spectroscopy analysis of whole cells and isolated cell walls of gram-positive bacteria: comparison with biochemical analysis. *J Bacteriol.* 1997;179:1023–8.
22. Vohrer U, Blomfield C, Page S, Roberts A. Quantitative XPS imaging – new possibilities with the delay-line detector. *Appl Surf Sci.* 2005;252:61–5.
23. Wang XJ, Haasch RT, Bohn PW. Anisotropic hydrogel thickness gradient films derivatized to yield three-dimensional composite materials. *Langmuir.* 2005;21:8452–9.
24. Tougaard S. Algorithm for automatic X-ray photoelectron spectroscopy data processing and X-ray photoelectron spectroscopy imaging. *J Vac Sci Technol A.* 2005;23:741–5.
25. Walton J, Fairley N. Quantitative surface chemical-state microscopy by X-ray photoelectron spectroscopy. *Surf Interface Anal.* 2004;36:89–91.
26. Walton J, Fairley N. Transmission-function correction for XPS spectrum imaging. *Surf Interface Anal.* 2006;38:388–91.
27. Steinmiller EMP, Choi K-S. Photochemical deposition of cobalt-based oxygen evolving catalyst on a semiconductor photoanode for solar oxygen production. *Proc Natl Acad Sci U S A.* 2009;106:20633–6.
28. Grünert W, Stakheev AY, Mörke W, Feldhaus R, Anders K, Shpiro ES, et al. Reduction and metathesis activity of  $\text{MoO}_3/\text{Al}_2\text{O}_3$  catalysts: I. An XPS investigation of  $\text{MoO}_3/\text{Al}_2\text{O}_3$  catalysts. *J Catal.* 1992;135:269–86.
29. Finster J, Klinkenberg ED, Heeg J, Braun W. ESCA and SEXAFS investigations of insulating materials for ULSI microelectronics. *Vacuum.* 1990;41:1586–9.
30. Casper L. Microelectronics processing: inorganic materials characterization. Washington DC: American Chemical Society; 1986.
31. Stingeder G. The challenge of microelectronics for analytical chemistry. *Fresenius J Anal Chem.* 1992;343:771–2.
32. Heung WF, Yang YP, Wong PC, Mitchell KAR, Foster T. XPS and corrosion studies on zinc phosphate coated 7075-T6 aluminium alloy. *J Mater Sci.* 1994;29:1368–73.
33. Windisch C, Baer D, Engelhard M, Jones R. Analyzing localized corrosion in ion-implanted metals via XPS/AES. *JOM J Miner Met Mater Soc.* 2001;53:37–41.
34. Chang MC, Tanaka J. XPS study for the microstructure development of hydroxyapatite-collagen nanocomposites cross-linked using glutaraldehyde. *Biomaterials.* 2002;23:3879–85.
35. Pan J, Thierry D, Leygraf C. Electrochemical and XPS studies of titanium for biomaterial applications with respect to the effect of hydrogen peroxide. *J Biomed Mater Res.* 1994;28:113–22.
36. Ratner B. Surface characterization of biomaterials by electron spectroscopy for chemical analysis. *Ann Biomed Eng.* 1983;11:313–36.
37. Walker AR. Charged particle energy analyser. US Patent: 4810879. 1989.



38. Paul EL, Michael AK. Surface charge neutralization of insulating samples in X-ray photoemission spectroscopy. *J Vac Sci Technol A*. 1998;16:3483–9.
39. Tougaard S. Universality classes of inelastic electron scattering cross-sections. *Surf Interface Anal*. 1997;25:137–54.
40. Hajati S, Tougaard S. XPS for non-destructive depth profiling and 3D imaging of surface nanostructures. *Anal Bioanal Chem*. 2010;396:2741–55.
41. Horbett TA, Brash JL. Proteins at interfaces II: fundamentals and applications. Washington D. C.: American Chemical Society; 1995.
42. Castner DG, Ratner BD. Biomedical surface science: foundations to frontiers. *Surf Sci*. 2002;500:28–60.
43. McArthur SL, McLean KM, Kingshott P, St John HAW, Chatelier RC, Griesser HJ. Effect of polysaccharide structure on protein adsorption. *Colloid Surf B-Biointerfaces*. 2000;17:37–48.
44. Salim M, O'Sullivan B, McArthur SL, Wright PC. Characterization of fibrinogen adsorption onto glass microcapillary surfaces by ELISA. *Lab Chip*. 2007;7:64–70.
45. Johnson G, Jenkins ML, McLean KM, Griesser HJ, Kwak J, Goodman M, et al. Peptoid-containing collagenmimetics with cell binding activity. *J Biomed Mater Res*. 2000;51:612–24.
46. Massia SP, Stark J. Immobilized RGD peptides on surface-grafted dextran promote biospecific cell attachment. *J Biomed Mater Res*. 2001;56:390–9.
47. Chow E, Wong ELS, Bocking T, Nguyen QT, Hibbert DB, Gooding JJ. Analytical performance and characterization of MPA-Gly-Gly-His modified sensors. *Sens Actuator B-Chem*. 2005;111:540–8.
48. Weidner T, Samuel NT, McCrear K, Gamble LJ, Ward RS, Castner DG. Assembly and structure of alpha-helical peptide films on hydrophobic fluorocarbon surfaces. *Biointerphases*. 2010;5:9–16.
49. Apte JS, Collier G, Latour RA, Gamble LJ, Castner DG. XPS and ToF-SIMS investigation of alpha-helical and beta-strand peptide adsorption onto SAMs. *Langmuir*. 2010;26:3423–32.
50. Feyrer V, Plekan O, Tsud N, Chab V, Matolin V, Prince KC. Adsorption of histidine and histidine-containing peptides on Au(111). *Langmuir*. 2010;26:8606–13.
51. Iucci G, Battocchio C, Dettin M, Gambaretto R, Polzonetti G. A NEXAFS and XPS study of the adsorption of self-assembling peptides on TiO<sub>2</sub>: the influence of the side chains. *Surf Interface Anal*. 2008;40:210–4.
52. Jedlicka SS, Rickus JL, Zemyanov DY. Surface analysis by X-ray photoelectron spectroscopy of sol–gel silica modified with covalently bound peptides. *J Phys Chem B*. 2007;111:11850–7.
53. Charnley M, Fairfull-Smith K, Haldar S, Elliott R, McArthur SL, Williams NH, et al. Generation of bioactive materials with rapid self-assembling resorcinarene-peptides. *Adv Mater*. 2009;21:2909–15.
54. Shen MC, Martinson L, Wagner MS, Castner DG, Ratner BD, Horbett TA. PEO-like plasma polymerized tetraglyme surface interactions with leukocytes and proteins: in vitro and in vivo studies. *J Biomater Sci-Polym Ed*. 2002;13:367–90.
55. Thissen H, Gengenbach T, du Toit R, Sweeney DF, Kingshott P, Griesser HJ, et al. Clinical observations of biofouling on PEO coated silicone hydrogel contact lenses. *Biomaterials*. 2010;31:5510–9.
56. Zinelis S, Thomas A, Syres K, Silikas N, Eliades G. Surface characterization of zirconia dental implants. *Dent Mater*. 2009;26:295–305.
57. Leitao E, Barbosa MA, deGroot K. XPS characterization of surface films formed on surface-modified implant materials after cell culture. *J Mater Sci-Mater Med*. 1997;8:423–6.
58. Liu YT, Li K, Pan J, Liu B, Feng SS. Folic acid conjugated nanoparticles of mixed lipid monolayer shell and biodegradable polymer core for targeted delivery of Docetaxel. *Biomaterials*. 2010;31:330–8.

59. Daniel C, Sohn KE, Mates TE, Kramer EJ, Radler JO, Sackmann E, et al. Structural characterization of an elevated lipid bilayer obtained by stepwise functionalization of a self-assembled alkenyl silane film. *Biointerphases*. 2007;2:109–18.
60. Kim HK, Kim K, Byun Y. Preparation of a chemically anchored phospholipid monolayer on an acrylated polymer substrate. *Biomaterials*. 2005;26:3435–44.
61. Michel R, Subramaniam V, McArthur SL, Bondurant B, D'Ambruoso GD, Hall HK, et al. Ultra-high vacuum surface analysis study of rhodopsin incorporation into supported lipid bilayers. *Langmuir*. 2008;24:4901–6.
62. McArthur SL, Halter MW, Vogel V, Castner DG. Covalent coupling and characterization of supported lipid layers. *Langmuir*. 2003;19:8316–24.
63. Russell BG, Moddeman WE, Birkbeck JC, Wright SE, Millington DS, Stevens RD, et al. Surface structure of human mucin using X-ray photoelectron spectroscopy. *Biospectroscopy*. 1998;4:257–66.
64. Lundin M, Sandberg T, Caldwell KD, Blomberg E. Comparison of the adsorption kinetics and surface arrangement of “as received” and purified bovine submaxillary gland mucin (BSM) on hydrophilic surfaces. *J Colloid Interface Sci*. 2009;336:30–9.
65. Libertino S, Giannazzo F, Aiello V, Scandurra A, Sinatra F, Renis M, et al. XPS and AFM characterization of the enzyme glucose oxidase immobilized on SiO<sub>2</sub> surfaces. *Langmuir*. 2008;24:1965–72.
66. Abbas A, Vercaigne-Marko D, Supiot P, Bocquet B, Vivien C, Guillochon D. Covalent attachment of trypsin on plasma polymerized allylamine. *Colloid Surf B-Biointerfaces*. 2009;73:315–24.
67. Debenedetto GE, Malitesta C, Zamboni CG. Electroanalytical X-ray photoelectron-spectroscopy investigation on glucose-oxidase adsorbed on platinum. *J Chem Soc-Faraday Trans*. 1994;90:1495–9.
68. Liu ZC, Zhang X, He NY, Lu ZH, Chen ZC. Probing DNA hybridization efficiency and single base mismatch by X-ray photoelectron spectroscopy. *Colloid Surf B-Biointerfaces*. 2009;71:238–42.
69. Zhang XC, Kumar S, Chen JH, Teplyakov AV. Covalent attachment of shape-restricted DNA molecules on amine-functionalized Si(111) surface. *Surf Sci*. 2009;603:2445–57.
70. May CJ, Canavan HE, Castner DG. Quantitative X-ray photoelectron spectroscopy and time-of-flight secondary ion mass spectrometry characterization of the components in DNA. *Anal Chem*. 2004;76:1114–22.
71. Petrovykh DY, Kimura-Suda H, Tarlov MJ, Whitman LJ. Quantitative characterization of DNA films by X-ray photoelectron spectroscopy. *Langmuir*. 2004;20:429–40.
72. Graf N, Gross T, Wirth T, Weigel W, Unger WES. Application of XPS and ToF-SIMS for surface chemical analysis of DNA microarrays and their substrates. *Anal Bioanal Chem*. 2009;393:1907–12.
73. Dhayal M, Ratner DA. XPS and SPR analysis of glycoarray surface density. *Langmuir*. 2009;25:2181–7.
74. Tyler BJ. XPS and SIMS studies of surfaces important in biofilm formation – three case studies. In: Prokop A, Hunkeler D, Cherrington AD, editors. *Bioartificial organs – science, medicine, and technology*. New York: New York Acad Sciences; 1997. p. 114–26.
75. Bejjani BA, Shaffer LG. Application of array-based comparative genomic hybridization to clinical diagnostics. *J Mol Diagn*. 2006;8:528–33.
76. Lamartine J. The benefits of DNA microarrays in fundamental and applied bio-medicine. *Mater Sci Eng C-Biomim Supramol Syst*. 2006;26:354–9.
77. Wu P, Castner DG, Grainger DW. Diagnostic devices as biomaterials: a review of nucleic acid and protein microarray surface performance issues. *J Biomater Sci-Polym Ed*. 2008;19:725–53.
78. Gong P, Harbers GM, Grainger DW. Multi-technique comparison of immobilized and hybridized oligonucleotide surface density on commercial amine-reactive microarray slides. *Anal Chem*. 2006;78:2342–51.

79. Leone L, Loring J, Sjooberg S, Persson P, Shchukarev A. Surface characterization of the Gram-positive bacteria *Bacillus subtilis* – an XPS study. *Surf Interface Anal.* 2006;38:202–5.
80. Rouxhet PG, Mozes N, Dengis PB, Dufrène YF, Gerin PA, Genet MJ. Application of X-ray photoelectron-spectroscopy to microorganisms. *Colloid Surf B-Biointerfaces.* 1994;2:347–69.
81. Tesson B, Genet MJ, Fernandez V, Degand S, Rouxhet PG, Martin-Jezequel V. Surface chemical composition of diatoms. *ChemBioChem.* 2009;10:2011–24.
82. Dague E, Delcorte A, Latge JP, Dufrène YF. Combined use of atomic force microscopy, X-ray photoelectron spectroscopy, and secondary ion mass spectrometry for cell surface analysis. *Langmuir.* 2008;24:2955–9.
83. Ojeda JJ, Romero-Gonzalez ME, Bachmann RT, Edyvean RGJ, Banwart SA. Characterization of the cell surface and cell wall chemistry of drinking water bacteria by combining XPS, FTIR spectroscopy, modeling, and potentiometric titrations. *Langmuir.* 2008;24:4032–40.
84. Boonaert CJP, Rouxhet PG. Surface of lactic acid bacteria: relationships between chemical composition and physicochemical properties. *Appl Environ Microbiol.* 2000;66:2548–54.
85. van der Mei HC, de Vries J, Busscher HJ. X-ray photoelectron spectroscopy for the study of microbial cell surfaces. *Surf Sci Rep.* 2000;39:3–24.
86. Sharma PK, Rao KH. Surface characterization of bacterial cells relevant to the mineral industry. *Miner Metall Process.* 2005;22:31–7.
87. Beech IB, Zinkevich V, Tapper R, Gubner R, Avci R. Study of the interaction of sulphate-reducing bacteria exopolymers with iron using X-ray photoelectron spectroscopy and time-of-flight secondary ionisation mass spectrometry. *J Microbiol Methods.* 1999;36:3–10.
88. Yuan SJ, Pehkonen SO. Microbiologically influenced corrosion of 304 stainless steel by aerobic *Pseudomonas NCIMB 2021* bacteria: AFM and XPS study. *Colloid Surf B-Biointerfaces.* 2007;59:87–99.
89. Sahrani FK, Aziz MA, Ibrahim Z, Yahya A. Surface analysis of marine sulphate-reducing bacteria exopolymers on steel during biocorrosion using X-ray photoelectron spectroscopy. *Sains Malays.* 2008;37:131–5.
90. Omoike A, Chorover J. Spectroscopic study of extracellular polymeric substances from *Bacillus subtilis*: aqueous chemistry and adsorption effects. *Biomacromolecules.* 2004;5:1219–30.
91. Rodrigues LR, Teixeira JA, van der Mei HC, Oliveira R. Isolation and partial characterization of a biosurfactant produced by *Streptococcus thermophilus* A. *Colloid Surf B-Biointerfaces.* 2006;53:105–12.
92. Fantauzzi M, Rossi G, Elsener B, Loi G, Atzei D, Rossi A. An XPS analytical approach for elucidating the microbially mediated enargite oxidative dissolution. *Anal Bioanal Chem.* 2009;393:1931–41.
93. Magnuson TS, Neal AL, Geesey GG. Combining in situ reverse transcriptase polymerase chain reaction, optical microscopy, and X-ray photoelectron spectroscopy to investigate mineral surface-associated microbial activities. *Microb Ecol.* 2004;48:578–88.
94. Kalinowski BE, Liermann LJ, Brantley SL, Barnes A, Pantano CG. X-ray photoelectron evidence for bacteria-enhanced dissolution of hornblende. *Geochim Cosmochim Acta.* 2000;64:1331–43.
95. Ahimou F, Boonaert CJP, Adriaensen Y, Jacques P, Thonart P, Paquot M, et al. XPS analysis of chemical functions at the surface of *Bacillus subtilis*. *J Colloid Interface Sci.* 2007;309:49–55.
96. Marshall KC, Pembrey R, Schneider RP. The relevance of X-ray photoelectron-spectroscopy for analysis of microbial cell-surfaces – a critical-view. *Colloid Surf B-Biointerfaces.* 1994;2:371–6.
97. Leone L, Ferri D, Manfredi C, Persson P, Shchukarev A, Sjöberg S, et al. Modeling the acid-base properties of bacterial surfaces: a combined spectroscopic and potentiometric study of the gram-positive bacterium *Bacillus subtilis*. *Environ Sci Technol.* 2007;41:6465–71.
98. Mine A, Yoshida Y, Suzuki K, Nakayama Y, Yatani H, Kuboki T. Spectroscopic characterization of enamel surfaces irradiated with Er: YAG laser. *Dent Mater J.* 2006;25:214–8.

99. Ziglo MJ, Nelson AE, Heo G, Major PW. Argon laser induced changes to the carbonate content of enamel. *Appl Surf Sci.* 2009;255:6790–4.
100. Busscher HJ, Vandermei HC, Genet MJ, Perdok JF, Rouxhet PG. XPS determination of the thickness of adsorbed mouthrinse components on dental enamel. *Surf Interface Anal.* 1990;15:344–6.
101. Taube F, Ylmen R, Shchukarev A, Nietzsche S, Noren JG. Morphological and chemical characterization of tooth enamel exposed to alkaline agents. *J Dent.* 2010;38:72–81.
102. Yoshida Y, Van Meerbeek B, Nakayama Y, Snauwaert J, Hellemans L, Lambrechts P, et al. Evidence of chemical bonding at biomaterial-hard tissue interfaces. *J Dent Res.* 2000;79:709–14.
103. Lou L, Nelson AE, Heo G, Major PW. Surface chemical composition of human maxillary first premolar as assessed by X-ray photoelectron spectroscopy (XPS). *Appl Surf Sci.* 2008;254:6706–9.
104. Andrade JD. X-ray photoelectron spectroscopy. In: Andrade JD, editor. *Surface and interfacial aspects of biomedical polymers.* New York: Plenum Press; 1985.
105. Burgos-Asperilla L, Garcia-Alonso MC, Escudero ML, Alonso C. Study of the interaction of inorganic and organic compounds of cell culture medium with a Ti surface. *Acta Biomater.* 2010;6:652–61.
106. Zelzer M, Alexander MR. Nanopores in single- and double-layer plasma polymers used for cell guidance in water and protein containing buffer solutions. *J Phys Chem B.* 2010;114:569–76.
107. Chung DJ. Surface modification of polymers for biomaterials. *J Dent Res.* 2001;80:1348.
108. Hartley PG, McArthur SL, McLean KM, Griesser HJ. Physicochemical properties of polysaccharide coatings based on grafted multilayer assemblies. *Langmuir.* 2002;18:2483–94.
109. Griesser HJ, Hartley PG, McArthur SL, McLean KM, Meagher L, Thissen H. Interfacial properties and protein resistance of nano-scale polysaccharide coatings. *Smart Mater Struct.* 2002;11:652–61.
110. Canavan HE, Cheng XH, Graham DJ, Ratner BD, Castner DG. Surface characterization of the extracellular matrix remaining after cell detachment from a thermoresponsive polymer. *Langmuir.* 2005;21:1949–55.
111. Artyushkova K, Fulghum JE. Multivariate image analysis methods applied to XPS imaging data sets. *Surf Interface Anal.* 2002;33:185–95.
112. Walton J, Fairley N. XPS spectromicroscopy: exploiting the relationship between images and spectra. *Surf Interface Anal.* 2008;40:478–81.
113. Artyushkova K. Structure determination of nanocomposites through 3D imaging using laboratory XPS and multivariate analysis. *J Electron Spectrosc Relat Phenom.* 2010;178:292–302.

Surface Analysis and Techniques in Biology

Smentkowski, V.S. (Ed.)

2014, X, 326 p. 157 illus., 83 illus. in color., Hardcover

ISBN: 978-3-319-01359-6